

Metallicity Discrepancy Between RGB and RHB Stars of the Globular Cluster M15

Jennifer Sobeck (ESO/Univ. of Texas), Robert Kraft (UCO Lick Obs.), and Chris Sneden (Univ. of Texas)



FIGURE: M15 (NGC 7078) is a slightly reddened ($E(B-V) = 0.10$), very metal-poor ($[Fe/H] \approx -2.4$) globular cluster. It has an integrated V magnitude of approximately 6.48 ($V = 6.48$) and specifically for its horizontal branch, $V_{HB} = 15.83$ (Harris 1996). The average age estimate for M15 is 12.3 Gyr (Sneden et al. 2000).

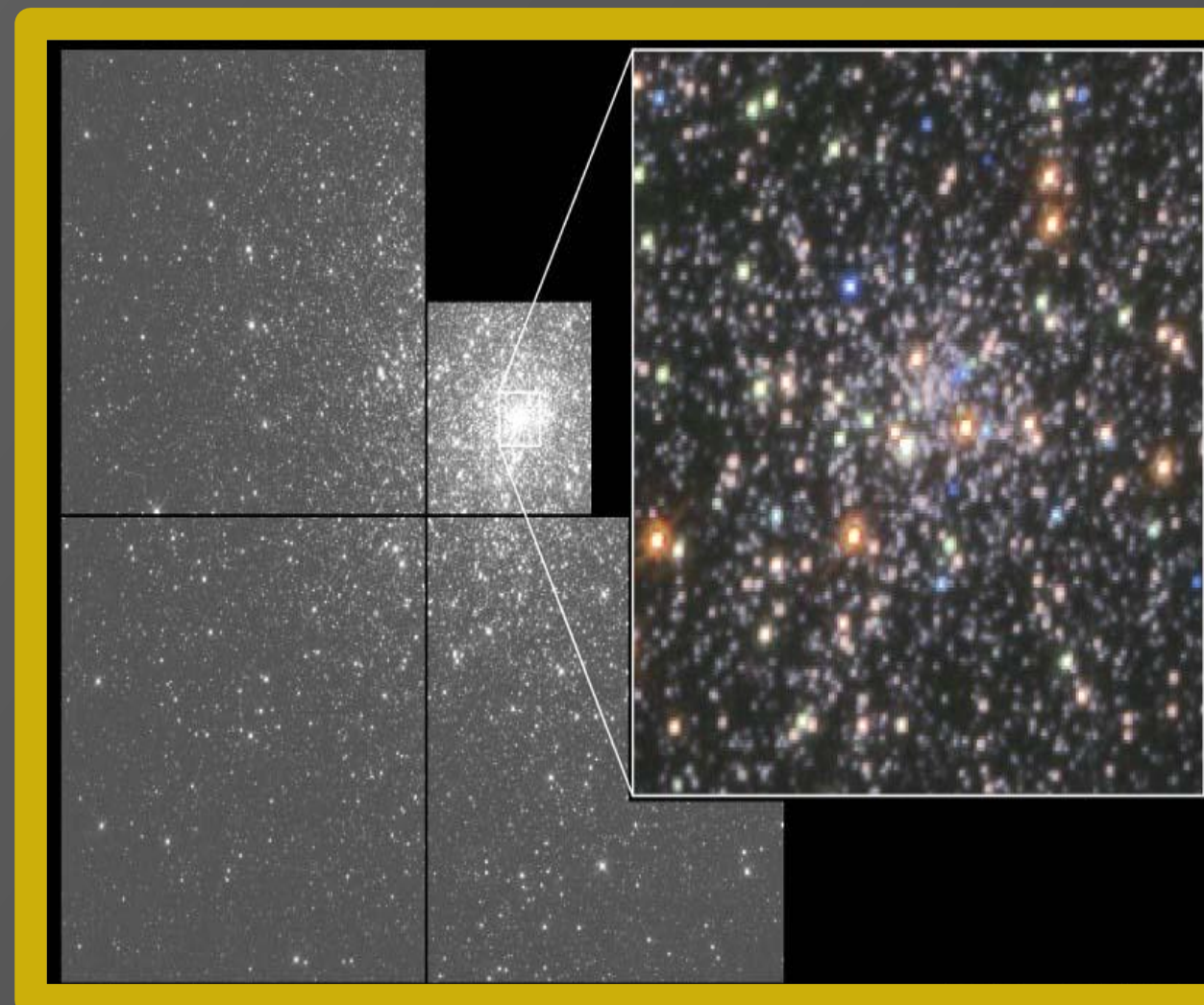


FIGURE: M15 is one of the most compact globular clusters (the denseness of M15 is a possible indicator of core collapse). Spitzer Space Telescope IRAC and MIPS observations confirm the presence of a planetary nebula (designated K468) and possibly detect the intracluster medium which would arise from mass-loss episodes from the evolved stellar population (Boyer et al. 2006).

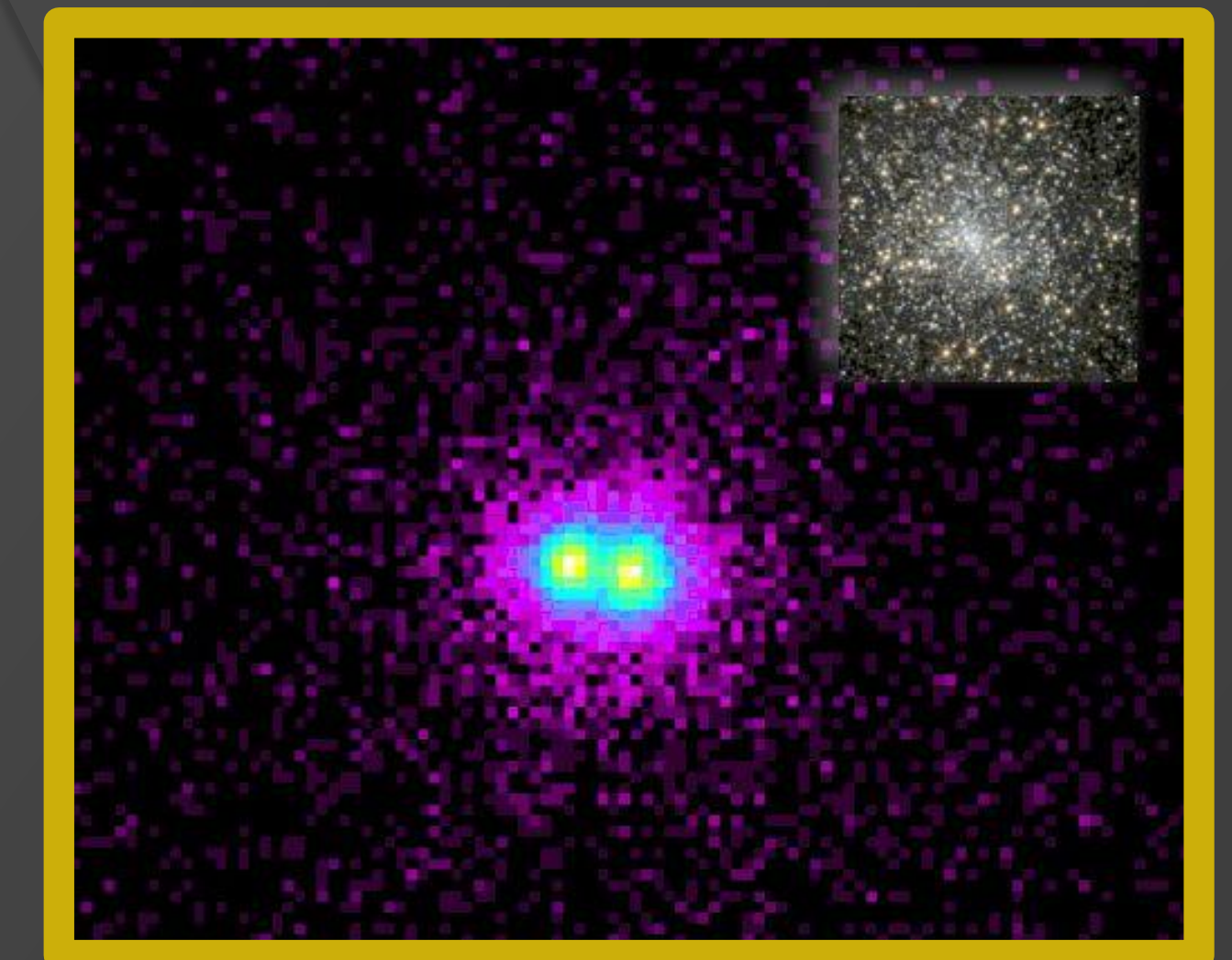


FIGURE: The false color Chandra Observatory image indicates two low-mass x-ray binary sources (in fact, one of these has an extraordinarily high luminosity optical counterpart; White & Angelini 2001). Four fainter x-ray sources have been identified within 50 arcsec of the core (two are cataclysmic variables; Hannikainen et al. 2005).

ABSTRACT: The surveys of Sneden et al. (1997, 2000) found star-to-star abundance scatter of the light elements and the neutron-capture elements in M15 Red Giant Branch (RGB) stars. Further examination of three select RGB tip stars revealed a distinct r-process nucleosynthetic signature (consistent with a scaled solar system r-process abundance distribution). As part of a general survey of metal-poor red horizontal branch (RHB) stars, Preston et al. (2006) observed six RHB members of M15. They detected some star-to-star abundance scatter in both the light and n-capture elements. However, Preston et al. found that the mean metallicity of these stars was significant lower (by roughly 0.2 dex) than their RGB counterparts. We present a new comparative abundance derivation for three RGB and six RHB stars of the globular cluster M15. We make a considerable effort to understand the apparent discrepancy in the metallicity of RGB and RHB stars. We then perform a detailed examination of the n-capture elements. We will discuss the abundance results and consider the chemical inhomogeneity of M15.

DATA SET DESCRIPTION: Acquisition of three red giant branch (RGB) stars spectra was done with (Sneden et al. 2000) with the High-Resolution Echelle Spectrograph at the Keck I telescope (Vogt et al. 1994). original observations of the M15 RHB stars (Preston et al. 2006) were obtained with the Magellan Ianmori Kyocera Echelle spectrograph at the Clay 6.5 m telescope at Las Campanas Observatory (Bernstein et al. 2003). Resolution of the two data sets were comparable: $R_{RGB} \approx 45,000$ and $R_{RHB} \approx 40,000$. For all spectroscopic observations, the S/N range was $30 < S/N < 260$. **Figure A** shows the stellar atmospheric parameters for all stars. The wavelength range of the data was roughly 3750-6800 Å. **Figure B** demonstrates that for blue wavelengths the Rayleigh scattering contribution becomes comparable to (and even exceeds) that from H_{-BF} for low temperature, low metallicity giants. In fact for the star of $T_{eff} = 4250$ K and $\log g = 0.50$, this figure shows that the opacity contribution from Rayleigh scattering outstrips that from H_{-BF} at wavelengths as red as $\lambda \approx 5000$ Å. Accordingly to accurately determine the line intensity with the correct amount of flux and opacity contribution, isotropic, coherent scattering must be taken into account.

TREATMENT OF SCATTERING: It was necessary to alter our spectral synthesis code MOOG (as it originally used a pure absorption source function ($S = \epsilon B$)) to incorporate a mean intensity (J) and a source function which sums both the absorption and scattering components ($S = \epsilon B + (1 - \epsilon)J$). Then, to solve the radiative transfer equation the Short Characteristics (SC) Methodology was employed. **Figure C** displays the Fe I abundances as a function of wavelength for the RGB star K341 ($T_{eff} = 4320$ and $\log g = 0.25$). In the upper panel and middle panels of **Figure C**, a least-squares fit to observed data (trendline) is shown. This trendline clearly indicates the degree to which the blue transitions bias the abundance results toward erroneously high values. The new version of MOOG which employs a more advanced radiative transfer approximation largely reduces the abundance trend with wavelength (upper versus middle panel). Also as expected, only the blue lines are substantially affected. **Figure D** is similar to **Figure C** except that Fe I abundances of the RHB star B412 ($T_{eff} = 6200$ and $\log g = 2.70$) are considered. No effect in the abundances is seen with the use of the new MOOG program. This is in line with expectations as B412 is a warmer, more dense star (and the H_{-BF} opacity contribution becomes large due to the increased electron pressure).

Star	Evolutionary State	T_{eff} [K]	$\log g$	$[M/H]$	v_t [km/s]
K341	RGB	4320	0.25	-2.20	2.20
K462	RGB	4320	0.25	-2.20	2.15
K583	RGB	4310	0.20	-2.20	2.30
B009	RHB	5300	1.65	-2.50	2.60
B028	RHB	5750	2.40	-2.50	2.85
B224	RHB	5600	2.10	-2.50	2.70
B262	RHB	4950	1.30	-2.50	1.90
B412	RHB	6200	2.70	-2.50	3.30
B584	RHB	6000	2.70	-2.50	2.90

FIGURE A

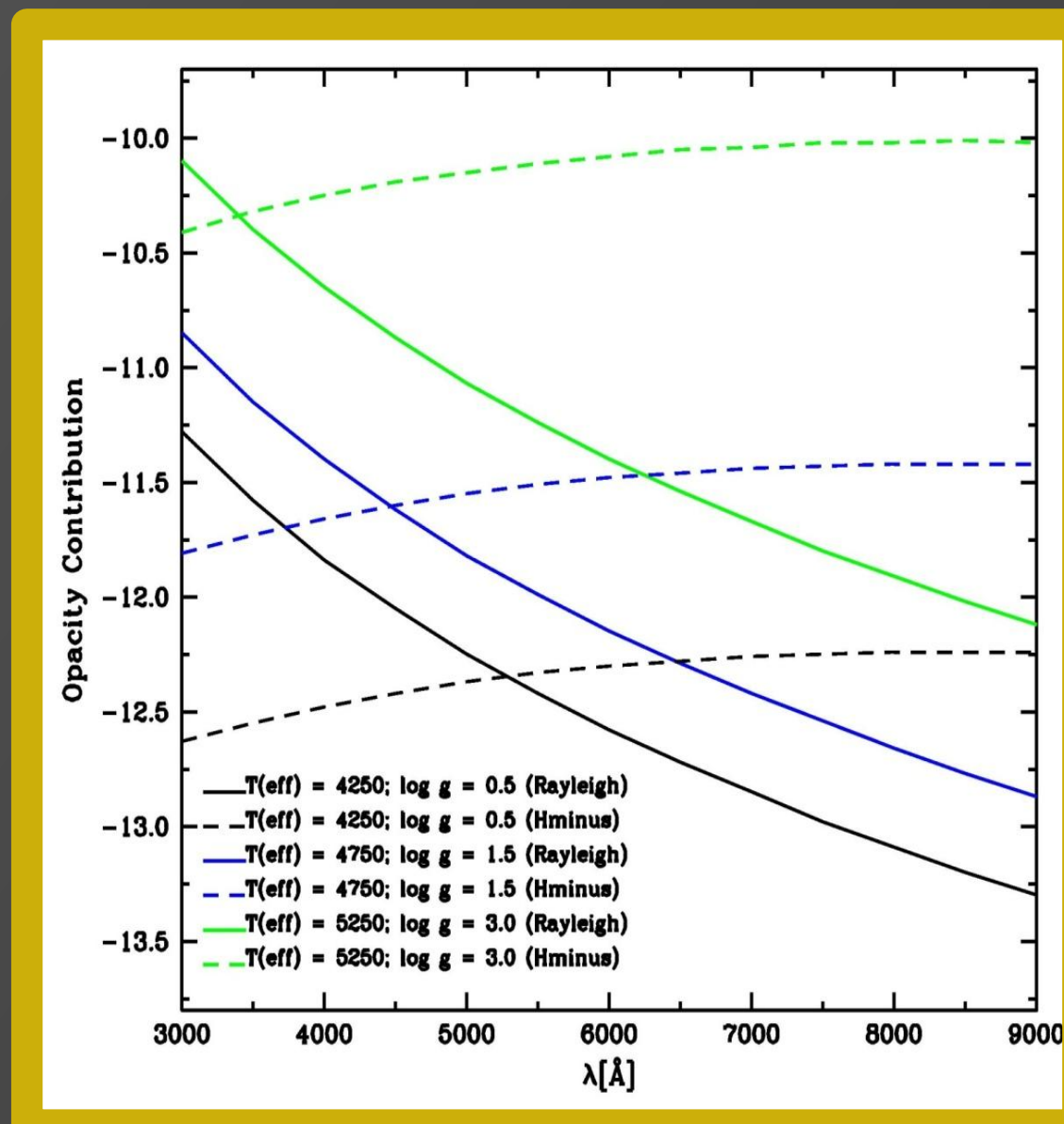


FIGURE B

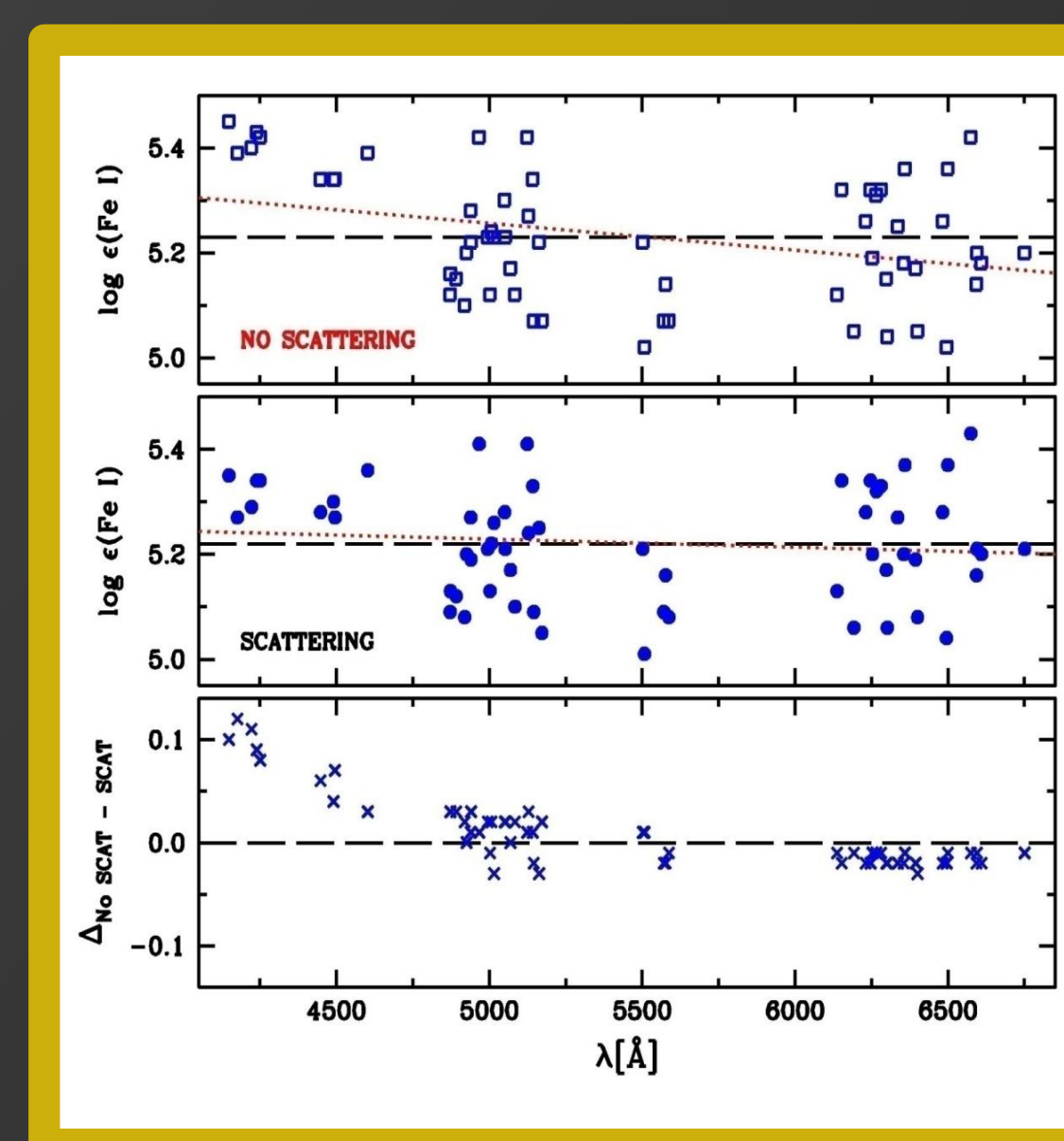


FIGURE C

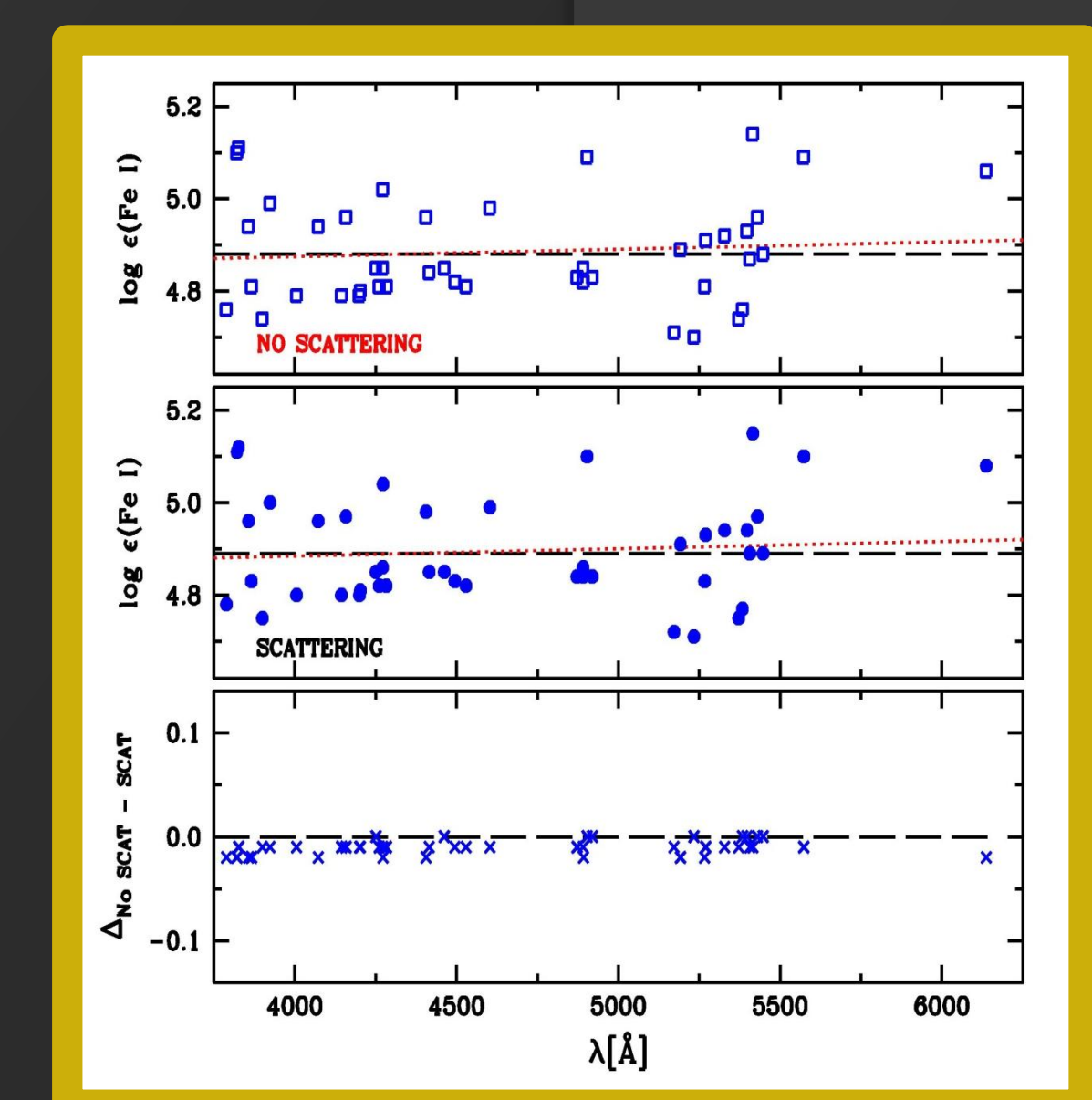


FIGURE D

DISCREPANCY IN IRON ABUNDANCE BETWEEN RGB AND RHB STARS: Mean iron abundances may be obtained for both sets of M15 stars: $\langle [Fe I/H] \rangle_{RGB} = 5.16$ ($\sigma = 0.07$) and $\langle [Fe II/H] \rangle_{RGB} = 5.15$ ($\sigma = 0.07$); and $\langle [Fe I/H] \rangle_{RHB} = 4.82$ ($\sigma = 0.06$) and $\langle [Fe II/H] \rangle_{RHB} = 4.87$ ($\sigma = 0.05$). The difference between the iron abundance of the RGB and RHB stars is approximately 0.30 dex and does not fall within the quadrature addition of the errors (0.09 dex). The employment of the new MOOG code did not affect the average RGB iron abundances (OLD-NEW = 0.01 for Fe I and OLD-NEW = -0.03 for Fe II). **Figure E** shows the average of the data set abundances (RGB or RHB) for each Fe I spectral feature and plots these values as a function of excitation potential (χ), oscillator strength ($\log(gf)$), and wavelength (λ). No definitive trend with any of the quantities is observed. **Figure F** is analogous to **Figure E** except that it shows $\log \epsilon$ (Fe II) versus χ , $\log(gf)$, and λ . The substantial disagreement between the RGB and RHB stars is not understood at this time.

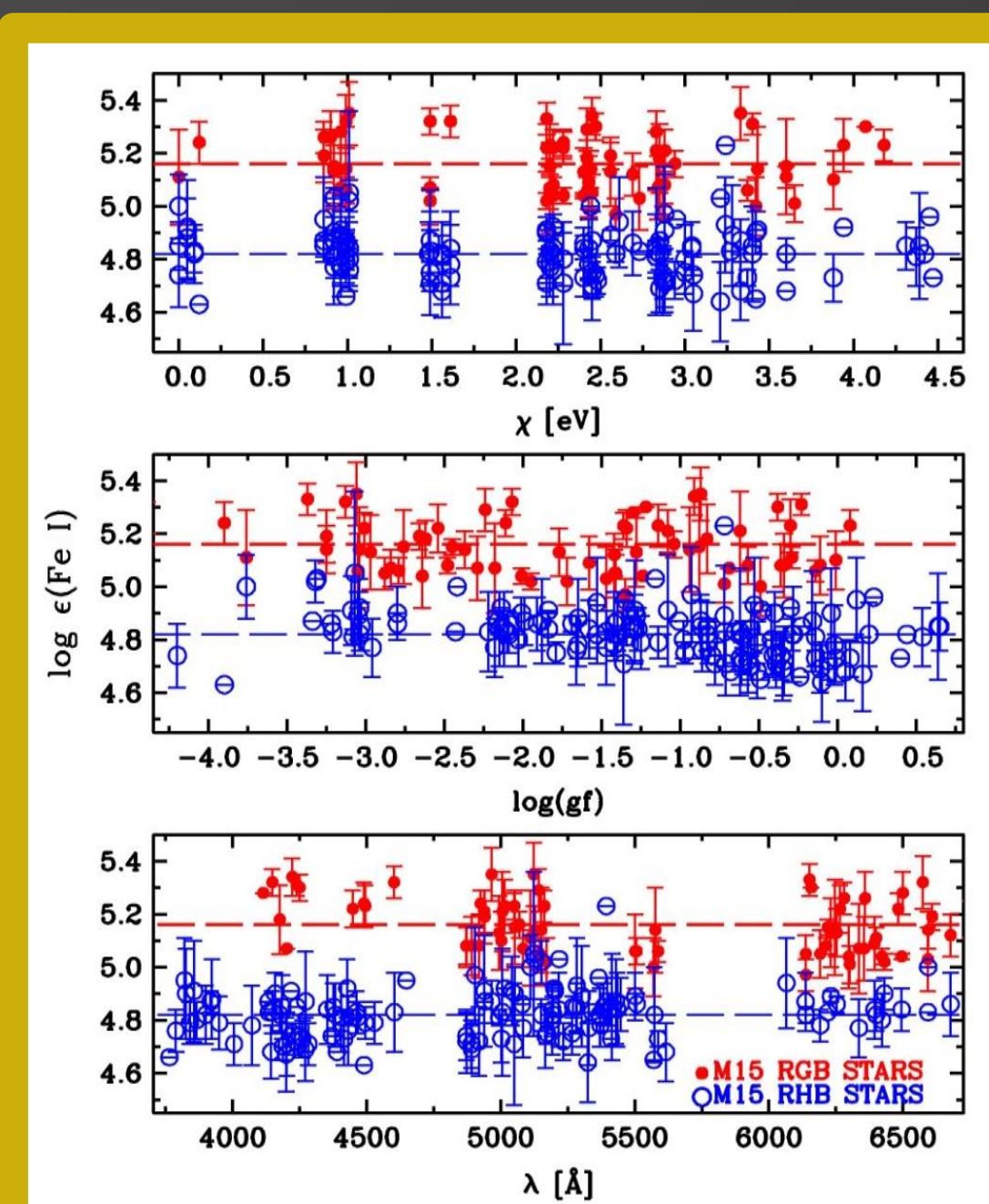


FIGURE E

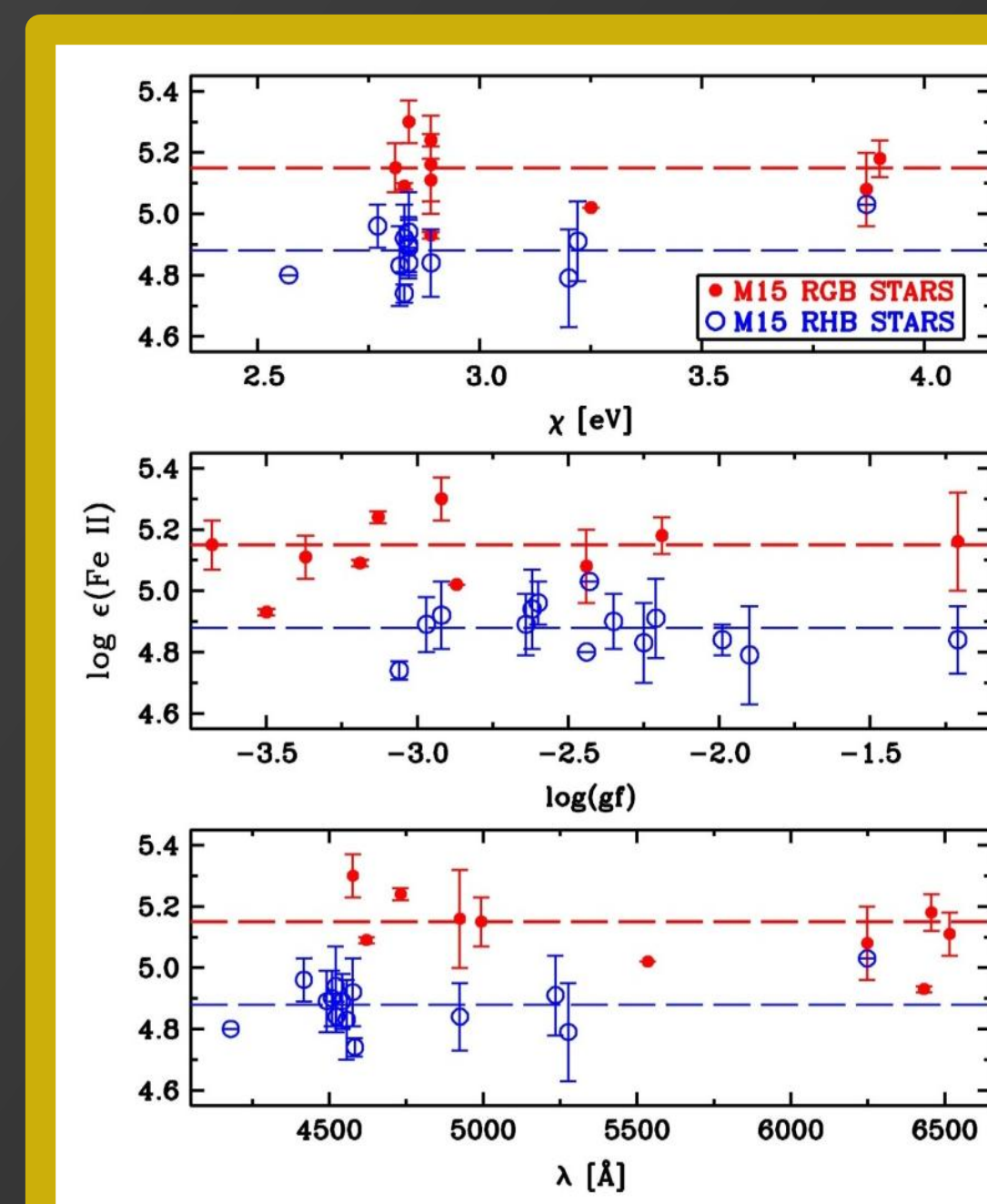


FIGURE F

NEUTRON CAPTURE ELEMENT ABUNDANCES: Figure G shows n-capture element abundances. The plot also includes the Otsuki et al. 2006 M15 RGB abundances. The one star that the Otsuki et al. and the present study have in common is indicated as a black dot encircled in red. **Figure H** displays the abundance as a function of atomic number for a few n-capture elements. All values are normalized to the average Nd abundance of the M15 RGB stars. The plot also includes the HD 221170 abundances from Ivans et al. (2006)

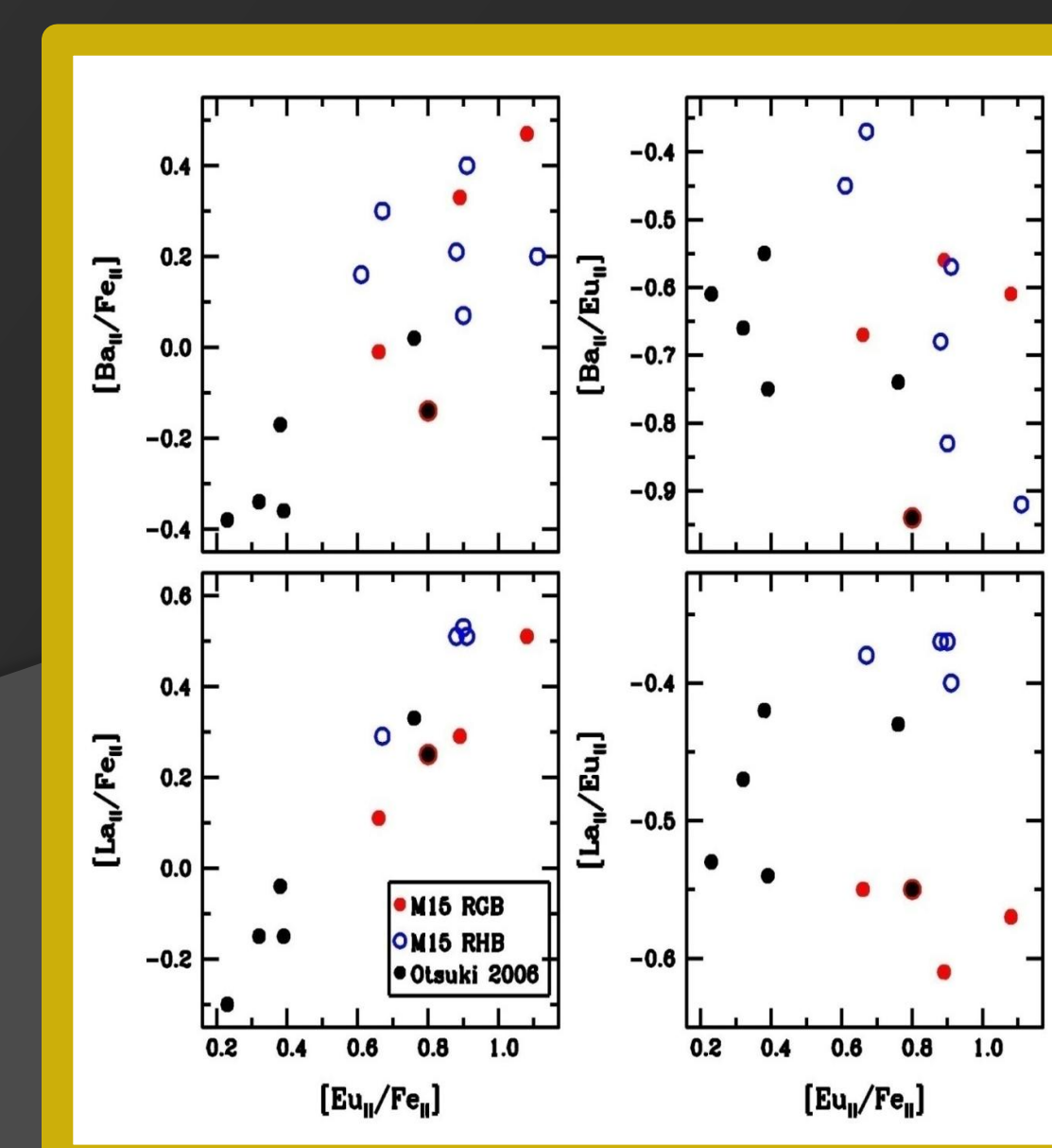


FIGURE G

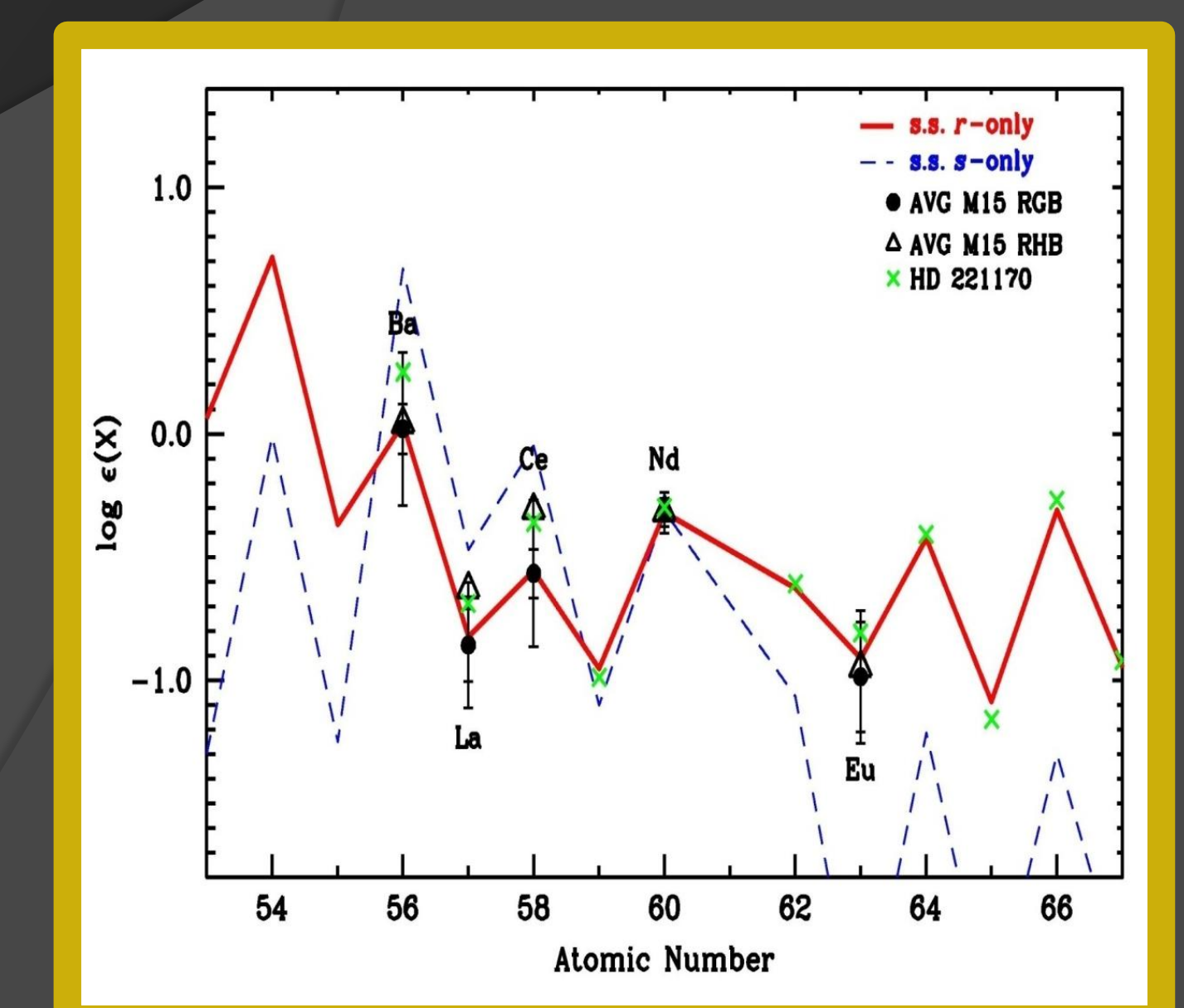


FIGURE H